Generalized extended Navier-Stokes theory: Multiscale spin relaxation in molecular fluids

J. S. Hansen

DNRF Centre "Glass and Time," IMFUFA Department of Nature, Systems and Models Roskilde University, DK-4000 Denmark

This paper studies the relaxation of the molecular spin angular velocity in the framework of generalized extended Navier-Stokes theory. Using molecular dynamics simulations, it is shown that for uncharged diatomic molecules the relaxation time decreases with increasing molecular moment of inertia per unit mass. In the regime of large moment of inertia the fast relaxation is wave-vector independent and dominated by the coupling between spin and the fluid streaming velocity, whereas for small inertia the relaxation is slow and spin diffusion plays a significant role. The fast wave-vector-independent relaxation is also observed for highly packed systems. The transverse and longitudinal spin modes have, to a good approximation, identical relaxation, indicating that the longitudinal and transverse spin viscosities have same value. The relaxation is also shown to be isomorphic invariant. Finally, the effect of the coupling in the zero frequency and wave-vector limit is quantified by a characteristic length scale; if the system dimension is comparable to this length the coupling must be included into the fluid dynamical description. It is found that the length scale is independent of moment of inertia but dependent on the state point.

I. INTRODUCTION

The coupling between the molecular spin angular velocity and the fluid streaming velocity has a significant impact on the fluid dynamics at small length scales. For example, for flows in nanochannels the coupling reduces the flow rate considerably due to the additional energy dissipation source coming from the molecules' spin [1]. It has also been shown that the coupling can act as a pumping mechanism [2,3] or as propellant for microrobots [4], even on large scales. In the dynamics of liquid crystals the coupling must be included to account for the dynamics [5].

Recently, Hansen *et al.* [6] extended the multiscale dynamical description of fluids to include the molecular spin angular velocity. This framework is termed generalized extended Navier-Stokes (GENS) theory, since it is based on the well-known extended Navier-Stokes equations [7–10] that include the dynamics of the molecular spin momentum. From the GENS formalism it is shown [6] that (i) the coupling between the molecular spin and the hydrodynamic degrees of freedom can be strictly ignored only in the hydrodynamic limit of zero wave vector; (ii) for chlorine fluid, the spin relaxation is wave-vector dependent for low densities but wave-vector independent at high densities, indicating that different mechanisms govern the relaxation for nonzero frequency and wave vector; and (iii) the longitudinal and transverse spin modes relax with approximately the same rate which differs substantially from the modes in the linear velocity field. Moreover, GENS theory enables a direct way to compute the rotational viscosity from equilibrium molecular dynamics simulations.

The purpose of this work is twofold. First, how spin relaxation is affected by varying the molecular moment of inertia per unit mass and fluid state point is studied. Second, a characteristic number is defined from the fluid transport coefficients at zero frequency and wave vector. This number quantifies the effect of the coupling. To carry out the investigation molecular dynamics (MD) simulations are used to simulate model fluids with different moment of inertia and at different state points.

GENS theory for uncharged systems is based on six fundamental correlation functions. In this work, we will focus on two of them, namely the transverse angular velocity autocorrelation function (TAVACF) and the longitudinal angular velocity autocorrelation function (LAVACF). These are defined as [6]

$$C_{\Omega\Omega}^{\perp}(\mathbf{k},t) = \langle \widetilde{\Omega}_z(\mathbf{k},t)\widetilde{\Omega}_z(-\mathbf{k},0)\rangle/V, \tag{1a}$$

$$C_{\Omega\Omega}^{\parallel}(\mathbf{k},t) = \langle \widetilde{\Omega}_y(\mathbf{k},t)\widetilde{\Omega}_y(-\mathbf{k},0)\rangle/V, \tag{1b}$$

where $\widetilde{\Omega}_z(\mathbf{k},t)$ and $\widetilde{\Omega}_y(\mathbf{k},t)$ are the Fourier components of the transverse and longitudinal spin angular velocity field. $\mathbf{k} = (0,k,0)$ is then the associated choice of wave vector, V is the system volume, and $\langle\ldots\rangle$ denotes the ensemble average. According to GENS theory, the TAVACF and LAVACF decay as [6]

$$C_{\Omega\Omega}^{\perp}(\mathbf{k},t) = C_{\Omega\Omega}^{\perp}(\mathbf{k},0)\exp\left[-\frac{4\eta_r + \zeta_t k^2}{\rho I}t\right] \text{ (small } k,I), \tag{2a}$$

$$C_{\Omega\Omega}^{\parallel}(\mathbf{k},t) = C_{\Omega\Omega}^{\parallel}(\mathbf{k},0)\exp\left[-\frac{4\eta_r + \zeta_l k^2}{\rho I}t\right] \text{ (small } k), \tag{2b}$$

where η_r is the rotational viscosity, ζ_t and ζ_l are the transverse and longitudinal spin viscosities all in the limit of zero wave vector and frequency, ρ is the mass density, and I the average moment of inertia per unit mass, here simply the molecular moment of inertia. According to Eq. (2) the decays are governed by two processes: a wave-vector-independent process which is due to the coupling to the linear momentum and a wave-vector-dependent diffusive process. From MD simulation of chlorine the TAVACF and LAVACF are indistinguishable except at very large wave vector at the fluid state point [6]. This indicates that $\zeta_t \approx \zeta_l$ for most systems. It is noted that the approximation Eq. (2a) is equivalent to ignoring the cross-correlation effects [6].

Importantly, Eq. (2) can be applied only to fluid composed of rigid uniaxial molecules. The general case requires inclusion of all relevant rotational axes and for flexible molecules even the dynamics of the moment-of-inertia tensor.

II. SIMULATION DETAILS

In what follows, all quantities are given in the usual MD (or Lennard-Jones) units [11]. Three series of simulations are carried out, series A, B, and C. In series A, a diatomic molecular fluid is simulated in the NpT ensemble at two state points, namely $(p,T) = (2.0, 1.0)$ and $(p,T) = (1.0, 5.0)$. First, the bond length l_b varies $0.25 \leqslant l_b \leqslant 1.00$, i.e., the moment of inertia per unit mass is changed. Second, mixtures of two different molecules are simulated to study the effect of dispersity. In series B, an asymmetric diatomic molecule is simulated in the NVT ensemble at different state points. The asymmetry arises due to the mass differences of the two constituent atoms; $m_1 = 1$ and $m_2 = 0.195$. The bond length is fixed at $l_b = 0.5841$. This molecular model is used as a model for liquid toluene. For series C, a diatomic molecule with bond length $l_b = 0.38$ is simulated in the NVT ensemble over a range of densities and at a fixed temperature, $T = 4.25$.

In all simulations, atoms not belonging to the same molecule interact via the cut and shifted Lennard-Jones potential [11],

$$U_{\mathrm{LJ}}(r_{ij}) = 4\left(r_{ij}^{-12} - r_{ij}^{-6}\right) + U_{\mathrm{LJ}}(r_c), \tag{3}$$

if $r_{ij} \leqslant r_c$, where r_{ij} is the distance between atoms i and j. In series A, the cutoff is set to $r_c = 2^{1/6}$, which is the purely repulsive WCA potential, whereas in B and C the cutoff is at $r_c = 2.5$. Bonds are flexible using a harmonic spring potential U_s, i.e., for two bonded atoms i and j,

$$U_s(r_{ij}) = \tfrac{1}{2}\, k_s (r_{ij} - l_b)^2, \tag{4}$$

with spring constant $k_s = 1000$ in A and $k_s = 3200$ in series B and C.

The equations of motion are integrated forward in time using a leap-frog algorithm with time step $h = 0.001$. The pressure and temperature are controlled with a Berendsen barostat and a Nose-Hoover thermostat (see Ref. [11]).

The wave-vector-dependent transverse angular velocity is found from

$$\widetilde{\Omega}_z(k,t) = \frac{3}{2\rho I} \sum_j s_{z,j}(t) \exp(-iky_j), \tag{5}$$

where y_j and $s_{z,j}$ are the y position and z component of the angular momentum of molecule j. The longitudinal angular velocity is likewise given by $\widetilde{\Omega}_y(k,t) = 3/(2\rho I) \sum_j s_{y,j}(t) \exp(-iky_j)$. See Ref. [6] for details. From these definitions the correlation functions can readily be evaluated. η_r and ζ_t are also computed in the limit of zero frequency and wave vector using the methods described in Refs. [6,10].

III. RESULTS AND DISCUSSION

Examples of the LAVACF and TAVACF for series A are shown in Fig. 1(a). For clarity, data for only one TAVACF is plotted, but all are within statistical uncertainty, as for the LAVACFs for the wave vectors studied here. The fact that the TAVACF and LAVACF follow the same relaxation confirms the relation $\zeta_l \approx \zeta_t$. We will from here onward denote the values of these viscosities using ζ.
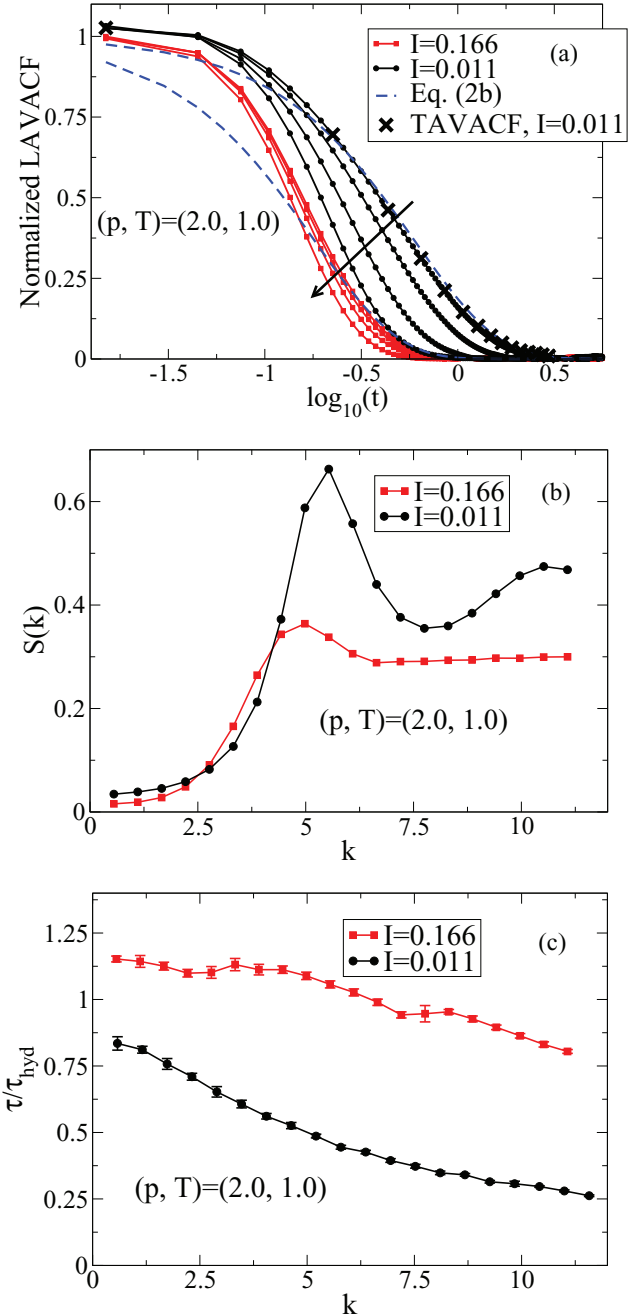
FIG. 1. (Color online) Results from series A. (a) Normalized LAVACF (filled circles) and TAVACF (crosses) versus time for four wave vectors $k = 0.55, 2.77, 4.98$, and 7.20. Arrow indicates trends for increasing wave vector. The dashed lines are the corresponding prediction of the GENS theory in the limit of zero wave vector and frequency. (b) Corresponding structure factor $S(\mathbf{k})$. (c) Normalized relaxation time as a function of wave vector. $\tau_{\mathrm{hyd}} = \rho I/(4\eta_r)$. Lines serve as a guide to the eye.

Recall that in Fig. 1 the pressure and temperature is fixed and only inertia, I, is varied. It is seen that the relaxation is faster for large inertia. The predictions from GENS theory for the lowest wave vector are plotted in Fig. 1(a) as dashed lines, where the frequency and wave-vector-independent transport coefficients are used, so no fitting has been carried out in

TABLE I. Results for series A. Values for the density and transport coefficients for $(p, T) = (2.0, 1.0)$. $\tau_{\mathrm{hyd}} = \rho I / (4\eta_r)$ and $l_c = \sqrt{\zeta/\eta_r}$; see text for details. The number density n is the molecular number density.

I	n	ρ	$\eta_r \times 10^2$	$\zeta \times 10^2$	τ_{hyd}	l_c
0.166	0.299	0.597	14 ± 1	23 ± 3	0.18	1.3
0.011	0.429	0.858	0.35 ± 0.04	0.7 ± 0.1	0.68	1.4

the comparison. The values for the density and transport coefficients are listed in Table I.

Importantly, increasing I results in a molecular number density (packing), n, decrease for a particular pressure; in series A $n \propto I^{-1}$. The relaxation is, thus, faster for lower packing, which contradicts usual viscous behavior as, for example, the shear viscosity increases dramatically for increasing densities. Figure 1(b) shows the corresponding structure factor (based on the molecules center of mass). For small I the fluid is more structured in accordance with the larger number density, i.e., structure cannot explain the faster dynamics observed for large moment of inertia. This indicates that the faster decay seen for large I is an inertia effect.

From the spin relaxation it is possible to determine a characteristic relaxation time τ. In the strict hydrodynamic limit the decay is wave-vector independent [see Eq. (2)], and one relaxation time can be expressed as $\tau_{\mathrm{hyd}} = \rho I / (4\eta_r)$. τ is, thus, defined as $C_{\Omega\Omega}^{\parallel}(\mathbf{k}, \tau) = \exp(-1) C_{\Omega\Omega}^{\parallel}(\mathbf{k}, 0)$. In Fig. 1(c) $\tau / \tau_{\mathrm{hyd}}$ is plotted as a function of wave vector. For large moment of inertia the relaxation is dominated by a wave-vector-independent process even for large wave vectors. This is surprising, considering the values for the viscosities in Table I. The result is interpreted as the rotational viscosity being frequency dependent and the spin viscosity to be both frequency and wave-vector dependent [6]. For large frequencies (fast relaxation) the dynamics is, thus, governed by the coupling process through η_r. Also, the fact that $\tau > \tau_{\mathrm{hyd}}$ is a result of the frequency dependence.

The moment of inertia entering the GENS theory is the average moment of inertia of the fluid. Thus, this quantity can also be varied by mixing molecules with different bond lengths. This introduces dispersity into the system and may result in a different fluid structure and dynamics. Two binary mixtures with molecules having $l_b = 0.25$ and $l_b = 1.0$ are studied. The fraction of the "smaller" molecule in the first mixture is 0.586 and 0.879 in the second mixture. This corresponds to $I = 0.075$ and $I = 0.029$. In Fig. 2 the LAVACF is plotted. It can be seen that the dynamics is faster for large I as the case for the single-component system. For large moment of inertia, the decay features smaller wave-vector dependence; this is also in agreement with the one-component situation. There is no indication of multiple dynamical modes due to different molecular relaxations. The structure factor (not shown) features a smooth transition between the two extremes shown in Fig. 1(b). It should be stressed that in the supercooled state, different dynamical relaxation times may be observed; however, this investigation is not the purpose of the current study.

The so-called strongly correlating liquids [12] feature isomorphs [13] in their phase diagram. Along an isomorph the
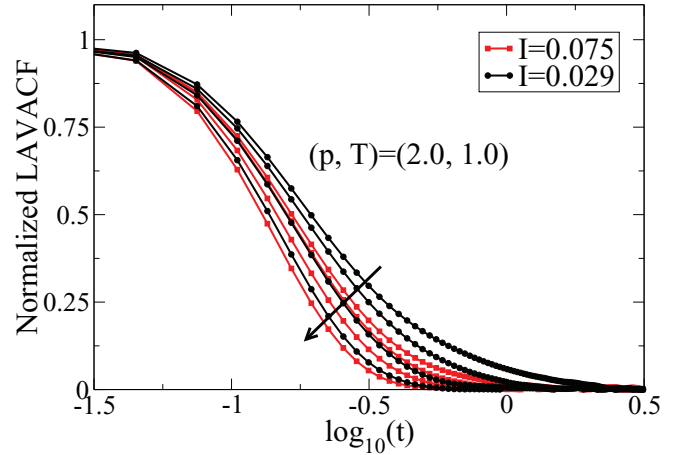
FIG. 2. (Color online) Normalized LAVACFs for fluid mixtures for four wave vectors $k = 0.55, 2.77, 4.98$, and 7.20. Arrow indicates trends for increasing wave vector. For clarity, a small time window is shown. Lines serve as a guide to the eye.

fluid has invariant structural and dynamical properties when expressed in appropriate reduced units; the reduced time is $t^* = tn^{1/3}\sqrt{k_B T/m}$), where m is the molecule mass and k_B is the Boltzmann constant. Figure 3 shows the LAVACF for the asymmetric dumbbell (series B) and for the four smallest wave vectors for two approximative isomorphic state points [14], $(\rho, T) = (0.9679, 0.480)$ and $(\rho, T) = (1.2189, 1.785)$. Note the reduced time on the x axis. For comparison, the isotherm state point $(\rho, T) = (0.9679, 1.785)$ is also shown. First, the LAVACF decays very fast at these dense packings (atomic number densities are 1.6184 and 2.04) and the spin momentum diffusion process is negligible, as discussed above. Second, the dynamics is clearly isomorphic invariant. It is here noted that the transverse velocity autocorrelation function (not shown) is also isomorphic invariant, highlighting the fact that not only is the multiscale rotational dynamics isomorphic invariant, so is the multiscale translational dynamics.
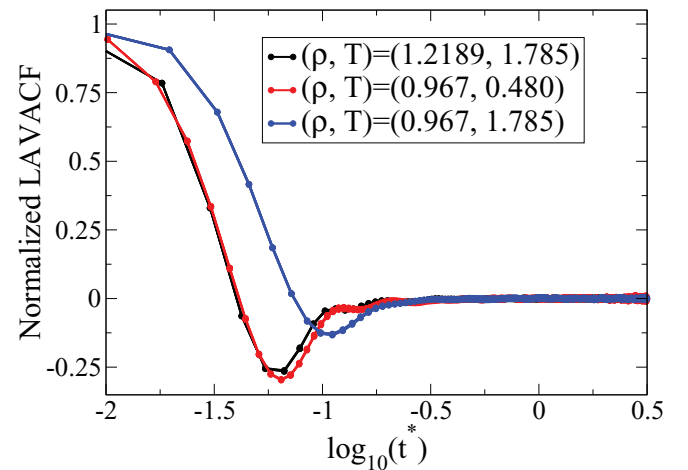
FIG. 3. (Color online) Results from series B. Normalized LAVACF for the four smallest wave vectors, $0.55 < k < 2.31$; the data points are so close that they cannot be distinguished. The reduced time, t^*, is given by $t^* = tn^{1/3}\sqrt{k_B T/m}$), where m is the mass and n is the molecular number density. Lines serve as guide to the eye.
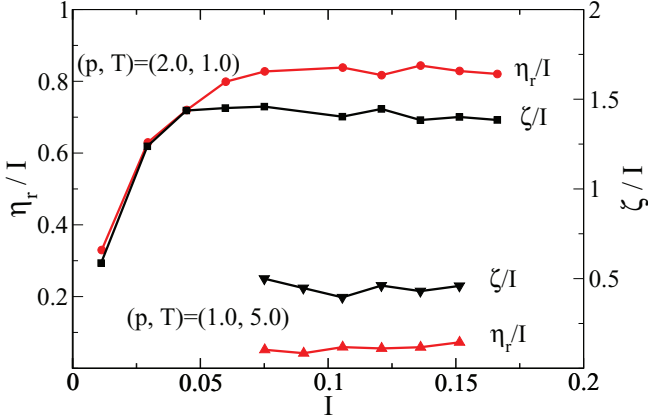
FIG. 4. (Color online) Results from series A. Rotational and spin viscosity as a function of moment of inertia in the zero frequency and wave-vector limit. The lines serve as a guide to the eye.

As discussed above, the rotational and spin viscosities are functions of the moment of inertia. In Fig. 4 the dependency is plotted for the two state points in series A. It is seen that for large I the viscosities are, to a good approximation, linear dependent of I. In the hydrodynamic regime, one can define a characteristic length scale l_c first discussed in Ref. [15] and given by

$$l_c(p,T) = \sqrt{\zeta/\eta_r}, \qquad (6)$$

which is independent of I. For the state point $(p,T) = (1.0, 5.0)$ we get $l_c \approx 2.0$ and for $(p,T) = (2.0, 1.0)$ $l_c \approx 1.5$. Using that $\rho \propto I^{-1}$, $\zeta = l_c^2 \eta_r$, and $\eta_r \propto I$ one can write the exponent in Eq. (2) as proportional to I, in agreement with the faster decay seen in Fig. 1(a). Bonthuis *et al.* [2] suggested that $\zeta = a^2 \eta_r$, where a is the molecule diameter, which must be estimated for nonspherical molecules. From the discussion above, this model cannot be strictly valid as the prefactor is dependent on the state point, something the intrinsic molecular details are not. Also, in general, we observe that $l_c > a$.

From Fig. 4 it is seen that l_c increases for decreasing pressure and increasing temperature. To explore this in detail, l_c is plotted as a function of density for all three simulation series, Fig. 5. Note that for the asymmetric molecule (series
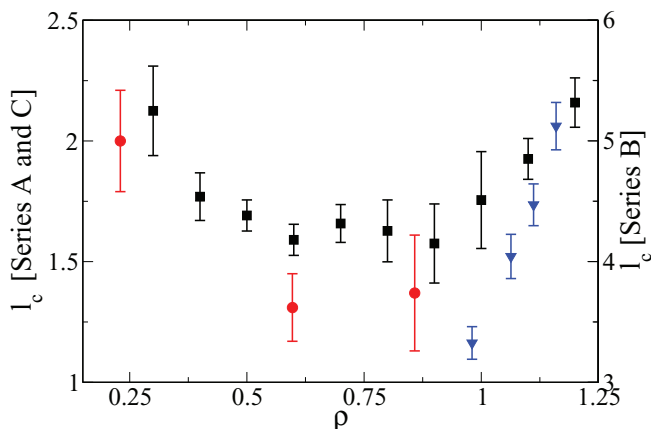
FIG. 5. (Color online) Characteristic length scale as a function of density for series A (circles), B (triangles), and C (squares).

B) results from isotherms are given. It is seen that l_c features a minimum for medium densities. This can be interpreted as follows: For low densities the kinetics dominates and the antisymmetric part of the stress determining η_r is small as this is arises from the configurational contributions. For large densities, the spin momentum diffusion is mostly governed by the couple forces which then grows faster than the antisymmetric part of the stress. It is worth noting that for highly packed fluids (series B) the characteristic length scale is large, meaning that the later suggested mechanism continues for increasing density.

Finally, it is in place to discuss the importance of l_c. For a steady (i.e., zero frequency) Poiseuille flow in a slit pore one can quantify a curvature by simple differentiation of the velocity profile at the center of the channel. Lower curvature corresponds to lower flow rate. The curvature can be calculated using the classical Navier-Stokes theory which ignores the spin dynamics and then by comparison with the predictions from extended Navier-Stokes theory. The relative difference between the two descriptions are given by [1]

$$C_{\mathrm{rel}} = 1 - \frac{\eta_r \coth(Kh)Kh}{(\eta_r + \eta_0)\cosh(Kh)}, \qquad (7)$$

where η_0 is the shear viscosity, $K = \sqrt{4\eta_r \eta_0/(\zeta[\eta_r + \eta_0])}$, and h is the pore half width. In the case of zero coupling, $\eta_r = 0$ and $C_{\mathrm{rel}} = 1$. Two limits are interesting here, namely

$$\lim_{l_c \to \infty} C_{\mathrm{rel}} = 1 - \eta_r/(\eta_r + \eta_0) \quad \text{and} \quad \lim_{l_c \to 0} C_{\mathrm{rel}} = 1. \qquad (8)$$

Equation (8) states that, in the hydrodynamic regime, there exists an upper limit to the effect of the diffusion of spin momentum and that, ignoring the diffusion, there is no effect of the coupling. For water at room temperature $l_c \approx 3.4$ nm [1,16]. Today, one can fabricate nanopores with widths of only 7 nm [17,18], so the coupling will have significant effects on the fluid flow rate in these highly confining geometries.

IV. CONCLUSION

In this paper, the spin relaxation of diatomic molecular fluids was studied. It was shown that the relaxation is dominated by the fast spin-velocity coupling process for large moment of inertia, I, and highly packed systems. For low moment of inertia, the slower spin-diffusion process plays a significant role in the relaxation despite the fact that the packing increases for a certain pressure and temperature. The longitudinal and transverse relaxation modes are identical, which means that the longitudinal and transverse spin viscosities have the same value.

In the hydrodynamic regime the rotational and spin viscosities are both linear dependent on I for sufficiently large inertia. This means that the characteristic length scale, l_c, is also independent of the moment of inertia, i.e., the spin-velocity coupling effect is unaltered by the moment of inertia. The characteristic length will, however, depend strongly on the state point featuring a minimum at medium densities.

[1] J. S. Hansen, P. J. Daivis, B. D. Todd, H. Bruus, and J. C. Dyre, Phys. Rev. E **84**, 036311 (2011).

[2] J. D. Bonthuis, D. Horinek, L. Bocquet, and R. R. Netz, Phys. Rev. Lett. **103**, 144503 (2009).

[3] S. De Luca, B. D. Todd, J. S. Hansen, and P. J. Daivis, J. Chem. Phys. **138**, 154712 (2013).

[4] B. U. Felderhof, Phys. Fluids **23**, 092003 (2011).

[5] H. Kneppe, F. Schneider, and N. K. Sharma, J. Chem. Phys. **77**, 3203 (1982).

[6] J. S. Hansen, P. J. Daivis, J. C. Dyre, B. D. Todd, and H. Bruus, J. Chem. Phys. **138**, 034503 (2013).

[7] H. Grad, Comm. Pure. Appl. Math. **5**, 455 (1952).

[8] S. R. de Groot and P. Mazur, *Non-equilibrium Thermodynamics* (Dover, London, 1984).

[9] N. K. Ailawadi, B. J. Berne, and D. Forster, Phys. Rev. A **3**, 1462 (1971).

[10] D. J. Evans and W. B. Streett, Mol. Phys. **36**, 161 (1978).

[11] M. P. Allen and D. J. Tildesley, *Computer Simulation of Liquids* (Clarendon Press, New York, 1989).

[12] U. R. Pedersen, T. Christensen, T. B. Schrøder, and J. C. Dyre, Phys. Rev. E **77**, 011201 (2008).

[13] N. P. Bailey, U. R. Pedersen, N. Gnan, T. B. Schrøder, and J. C. Dyre, J. Chem. Phys. **129**, 184508 (2008).

[14] D. E. Albrechtsen (unpublished).

[15] J. S. Hansen, P. J. Daivis, and B. D. Todd, Phys. Rev. E **80**, 046322 (2009).

[16] J. S. Hansen, Henrik Bruus, B. D. Todd, and Peter J. Daivis, J. Chem. Phys. **133**, 144906 (2010).

[17] F. Martin, R. Walczak, A. Boiarski, M. Cohen, T. West, C. Cosentino, and M. Ferrari, J. Control. Release **102**, 123 (2005).

[18] L. H. Thamdrup, F. Persson, H. Bruus, H. K. Flyvbjerg, and A. Kristensen, Appl. Phys. Lett. **91**, 163505 (2007).